FFI Norwegian Defence Research Establishment

24/00884

FFI-RAPPORT

An operational dispersion model for wind over swell seas

Espen Åkervik
Andreas Nygård Osnes

An operational dispersion model for wind over swell seas

Espen Åkervik
Andreas Nygård Osnes

Norwegian Defence Research Establishment (FFI) 4 July 2024

Keywords
Turbulens
Bølger
Computational Fluid Dynamics (CFD)

FFI report
24/00884

Project number
1575

Electronic ISBN
978-82-464-3541-1

Approvers
Anders Helgeland, *Research Manager*
Morten Aronsen, *Acting Director of Research*

The document is electronically approved and therefore has no handwritten signature.

Summary

In this report, we develop an operational contaminant transport model suitable for offshore conditions. Although the model is, in principle, independent of sea state, we expect it to be most useful for swell sea calculations, that is, for long and fast waves.

The model is based on tracking of Lagrangian particles with turbulent motion stemming from a random walk procedure. As in standard operational models, the mean wind is given as a simple logarithmic vertical profile.

In this model, the novel element is the addition of quasi-laminar wave-correlated forcing. In order to properly model the influence of waves on the flow of the atmospheric boundary layer, it is generally necessary to utilize high fidelity computational fluid dynamics models (CFD models). These models lead to computationally demanding simulations, which makes them infeasible for operational dispersion modeling. For a less demanding alternative, we extend the laboratory-scale framework proposed by Åkervik and Vartdal in "The role of wave kinematics in turbulent flow over waves" (2019) to create a simple flow model on an operational scale, in other words on spatial scales ranging from meters to kilometers. This model does not fully model the influence of waves on the flow, but we believe that it covers the most important features from a dispersion point of view. The resulting dispersion problem can be solved on a regular computer in minutes.

We develop and test our transport model on a laboratory scale, for which we have high-fidelity reference data. Thereafter, we extend the model to full scale and compare it with a Gaussian puff model as well as published high-fidelity data. We demonstrate that the model yields reasonable results and that it can describe the effect of swell waves on the dispersion of aerosols.

Samandrag

I denne rapporten utviklar vi ein operasjonell modell for transport av farestoff til havs. I prinsippet skal modellen fungere for alle sjøtilstandar, men vi forventar at han er mest nyttig for berekningar med dønningar, altså for lange og raske bølger.

Modellen er basert på ein partikkelmetode der turbulente rørsler vert modellerte ved hjelp av ein såkalla tilfeldig gonge-metode (random-walk). Akkurat som i dei fleste operative spreiingsmodellar bruker vi ein enkel analytisk vertikalprofil til å skildre middelvinden.

Det nyskapende elementet i modellen er at partiklane vert påverka av ei kvasilaminær bølgekorrelert kraft. Dersom ein hadde hatt som mål å modellere alle aspekt av påverknaden til bølgene på det atmosfæriske grensesjiktet, ville ein måtte bruke ein høgkvalitets numerisk fluiddynamikkmodell (computational fluid dynamics-modell - CFD-modell). Bruken av slike modellar fører til særs krevjande berekningar, noko som gjer dei ueigna til operasjonell spreiingsmodellering. For å unngå dette utvidar vi rammeverket til Åkervik og Vartdal i "The role of wave kinematics in turbulent flow over waves" (2019) til å skape ein enkel strømningsmodell på operasjonell skala, altså på romlege skalaer frå meter til kilometer. Modellen fangar ikkje fullt ut påverknaden frå bølgene på straumdraget, men frå et spreiingsperspektiv meiner vi at han inneheld dei viktigaste effektane. Det resulterande spreiingsproblemet kan løysast på ei vanlig datamaskin på få minutt.

Vi utviklar og testar transportmodellen vår på laboratorieskala, der vi har referansedata med høg nøyaktigheit. Deretter utvidar vi modellen til full skala og samanliknar han med ein gaussisk puff-modell og med publiserte data som stammar frå ein veggmodellert storvirvelmodell. Vi demonstrerer at modellen gir rimelege resultat, og at han kan skildre effekten frå dønningane på spreiinga av aerosolar.

Contents

1 Introduction

Accidents on offshore structures or ships can cause releases of hazardous materials into the atmosphere. To understand the risks related to such events, one would like to know how quickly a material will be transported with the wind, how high concentrations that will be found at a certain distance, and how much of the material will be deposited into the water. These data can be obtained with the aid of computational models, provided that they capture the relevant physical processes involved in atmospheric dispersal at sea.

From a dispersion point of view, particles and/or gases are predominantly transported with the mean wind, $U(z)$, which is a function of height z. Turbulence creates an extra transport (or mixing) mechanism through the action of so-called eddies, which is often described as a type of diffusion, although it is purely kinematic (Taylor, 1922). In dispersion modeling, this effect is most famously characterized by Gaussian plume and puff models (Hanna et al., 1977). Since offshore wind conditions are reminiscent of those over smooth surfaces onshore, there is every reason to expect that the so-called Gaussian models can describe the dispersion patterns offshore. However, water waves add an extra component to the wind, which leads to altered vertical fluxes (Sullivan and McWilliams, 2010). This effect may lead to additional vertical lift of the plume (Li et al., 2019) and enhancement or prevention of deposition (Åkervik, 2022), thus altering the concentrations. Except for the two previous references, these effects appear to be overlooked by the research community (Åkervik and Gjesdal, 2023).

The flow over waves is a difficult problem from a computational perspective, and requires the coupling of a model for the propagation of waves and a model for the flow of air (Deskos et al., 2021). Even the air flow response to a prescribed propagating wave is difficult to model. The main challenge is the same as in the standard wall bounded turbulent flow, namely the huge separation of scales, ranging from microns to several kilometers. For the flow over a flat rough surface, the research community has successfully used the so called Monin-Obukhov similarity theory (Foken, 2006), which is a one-dimensional stress description of the boundary layer. The concept of surface roughness is central to this description. Onshore, roughness lengths are given by the type of surface present, for instance grass lands, bushes, sand dunes and snow cover. Offshore, the roughness has traditionally either been set very low or one has used the so called Charnocks rule, which prescribes larger roughness lengths as the mean wind speed increases. Although commonly used in meteorological models, this framework is not expected to be valid for swell sea (Sullivan and McWilliams, 2010).

In order to achieve flow solutions on a reasonable scale, wall modelled Large eddy simulation models (WMLES) have recently been developed and tested on the flow over waves. These models are promising, but are at the present computationally expensive and appears to be cumbersome to implement in existing Computational fluid dynamics (CFD) solvers (see for instance Yang et al., 2013a,b, to appreciate the complexity).

As an alternative to the complicated and time-consuming Large-eddy simulation (abbreviated as LES, see for instance Versteeg and Malalasekera, 2007) models, we here build an operational scale contaminant transport model that can be solved in minutes on a standard computer. The main parts of the model is

- Vertical one-dimensional mean flow and turbulence profiles augmented by two-dimensional

wave correleated flow fields obtained from the framework of Åkervik and Vartdal (2019). This is in the spirit of Hussain and Reynolds (1970, 1972), who introduced a triple decomposition (mean flow, turbulent stresses, and wave correlated stresses).

- A Lagrangian particle tracking method with a random walk method to incorporate the effect of turbulence.

The framework of Åkervik and Vartdal (2019) was not suitable as a standalone model, since it relied on exact turbulent stresses. Here, we introduce eddy viscosity closures (see for instance Durbin and Reif, 2011), which enables the model to be used as a normal Reynolds averaged Navier-Stokes (RANS) type of model suitable for both laboratory scales and operational scales.

The report is organized as follows. In chapter 2, the Lagrangian particle method is described. The flow models are described in chapter 3. In chapter 4, we show the basic laminar transport mechanisms, and chapter 5 deals with the validation on laboratory scales. The model is extended to operational scales in chapter 6, and some conclusions are drawn in chapter 7.

2 A particle based contaminant transport model

We seek to describe the dispersion problem of how the concentration of a contaminant varies in space and time after a release. This concentration can be written $c(x, y, z, t)$, where x, y, and z are the three spatial directions and t is time. The dispersion problem can be written as an advection diffusion equation for the scalar field c, but it may also be written as a particle transport problem. In this case, the concentration must be computed from the average distance between individual particles (c.f Åkervik, 2022).

Generally, particles are subject to many forces (Schwarzkopf et al., 2012), but in this report we consider only drag forces and gravity. The equations governing the motion of a particle are then

$$\frac{\mathrm{d}\mathbf{x}_p}{\mathrm{d}t} = \mathbf{u}_p, \tag{2.1}$$

$$\frac{\mathrm{d}\mathbf{u}_p}{\mathrm{d}t} = \frac{C_d}{\tau_{\mathrm{St}}}\left(\mathbf{u} - \mathbf{u}_p\right) - \left(1 - \rho/\rho_p\right)\mathbf{g}, \tag{2.2}$$

where $\frac{\mathrm{d}\cdot}{\mathrm{d}t}$ denotes time derivative, $\mathbf{x}_p = (x_p, y_p, z_p)^T$ the particle position, $\mathbf{u}_p = (u_p, v_p, w_p)^T$ the particle velocity, $\mathbf{u} = (u, v, w)^T$ the flow velocity, and ρ and ρ_p the fluid and particle densities, respectively. Gravity points in the z-direction so that $\mathbf{g} = (0, 0, -9.81\mathrm{m/s}^2)$. The Stokes timescale τ_{St} is given as

$$\tau_{\mathrm{St}} = \frac{\rho_p d_p^2}{18\mu}, \tag{2.3}$$

and roughly gives the time it takes for a particle to adjust to the flow velocity in a very viscous fluid. For a characteristic time scale of the flow (denoted τ_{Flow}) we may define the Stokes number as

$$\mathrm{St} = \frac{\tau_{\mathrm{St}}}{\tau_{\mathrm{Flow}}}. \tag{2.4}$$

We use the same drag law as Bocksell and Loth (2001),

$$C_d = \left(1 + \frac{1}{6} Re_p^{2/3}\right), \quad \text{where} \quad Re_p = \frac{\rho |\mathbf{u} - \mathbf{u}_p| d_p}{\mu}. \tag{2.5}$$

Turbulence implicitly enters the expression through $\mathbf{u}$. A general turbulent flow field can be written as the Reynolds decomposed flow field (Pope, 2000) at the particle position $\mathbf{x}_p$

$$\mathbf{u}(\mathbf{x}_p, t) = \mathbf{U}(\mathbf{x}_p) + \mathbf{u}'(\mathbf{x}_p, t), \tag{2.6}$$

where $\mathbf{U}(\mathbf{x}_p)$ is the space dependent mean flow and $\mathbf{u}'(\mathbf{x}_p, t)$ is the zero mean turbulent fluctuations that varies in time and space. In general, for offline random walk, we only have access to the mean flow, regardless of whether experimental or numerical data is used. Capturing the effect of turbulence in a random walk model therefore involves synthetically generating turbulent fluctuations that preserves the statistical properties of the measured or modelled flow. The Continous Random Walk method (Bocksell and Loth, 2001) has been used successfully for this purpose for other flow regimes. This framework can be derived from the Langevin equation and leads to a discrete system in the form of a Markow chain (Pope, 1994). We follow Bocksell and Loth (2006) and write the Markow chain update of the syntetic turbulence field as

$$\mathbf{u}'(t + h) = \mathcal{G}\mathbf{u}'(t) + H\xi(t) + \mathbf{u}_{\text{drift}} \frac{1}{1 + \text{St}_{\text{turb}}}, \tag{2.7}$$

where $\mathcal{G}$ and H are 3×3 diagonal matrices and $\mathbf{u}_{\text{drift}} = \left(0,\ 0,\ h\frac{\mathrm{d}\sigma_w^2}{\mathrm{d}z}\right)$ is a so called drift correction to avoid unphysical clustering of finite sized particles in low-turbulence regions (Bocksell and Loth, 2006). The drift correction is tapered off for high inertia particles through the Stokes correction factor $1/(1 + \text{St}_{\text{turb}})$, where St_{turb} is the ratio of the particle relaxation time scale (τ_{St}) and the turbulence integral time scale (τ_{int}), *i.e.* $\text{St}_{\text{turb}} = \tau_{\text{St}}/\tau_{\text{int}}$. Randomness is introducted through the vector $\xi(t)$, which contains three independent random variables drawn from a normal distribution with zero mean and unity variance. In $\mathcal{G}$, the diagonal elements are $(k_u,\ k_v,\ k_w)$, where

$$k_u = \exp\left(-h/\tau_{\text{int}}^u\right), \quad k_v = \exp\left(-h/\tau_{\text{int}}^v\right), \quad \text{and} \quad k_w = \exp\left(-h/\tau_{\text{int}}^w\right). \tag{2.8}$$

In H, the diagonal elements are

$$\left(\sigma_u\sqrt{1 - k_u},\ \sigma_v\sqrt{1 - k_v}, \sigma_w\sqrt{1 - k_w}\right), \tag{2.9}$$

where the Reynolds stress terms are:

$$\sigma_u^2 = \overline{u'u'}, \quad \sigma_v^2 = \overline{v'v'}, \quad \text{and} \quad \sigma_w^2 = \overline{w'w'}. \tag{2.10}$$

The turbulent kinetic energy is given as $k = \frac{1}{2}(\sigma_u^2 + \sigma_v^2 + \sigma_w^2)$. All variables are evaluated at the particle position. The equation system must be closed by supplying models for the turbulent stresses and turbulent time scales.

The final particle model can then be written for first order forward finite differences as:

$$\mathbf{q}(t + h) = \mathbf{q}(t) + hf(\mathbf{q}), \quad \text{finite difference form of} \quad \frac{\mathrm{d}\mathbf{q}}{\mathrm{d}t} = f(\mathbf{q}), \tag{2.11}$$

where $\mathbf{q}(t) = (\mathbf{x}_p(t), \mathbf{u}_p(t), \mathbf{u}'(t))^T$ and

$$f(\mathbf{q}) = \begin{pmatrix} \mathbf{u}_p \\ \frac{C_d}{\tau_{\text{St}}}\left(\mathbf{U}(\mathbf{x}_p) - \mathbf{u}'(t) - \mathbf{u}_p(t)\right) - h\left(1 - \rho/\rho_p\right)\mathbf{g} \\ \left((\mathcal{G} - 1)\mathbf{u}'(t) + \mathcal{H}\xi(t) + \mathbf{u}_{\text{drift}}\frac{1}{1+\text{St}_{\text{turb}}}\right)/h \end{pmatrix}. \tag{2.12}$$

3 Flow models

3.1 Wave flow model

In order to fully describe the flow over waves, high fidelity models in the form of LES or RANS are needed (Sullivan and McWilliams, 2010). However, this comes at the price of high computational cost. To simplify the problem we state the following:

- We only need a rough description of the mean flow as it relates to friction velocity and roughness length. For this purpose, the Monin-Obukhov framework (Foken, 2006)[1] with Charnocks formula for roughness will suffice (Charnock, 1955).
- From the wind-wave interaction we only utilize the wave correlated laminar velocities. We therefore omit knowledge of the wave correlated turbulent velocities, and hope that they are of less importance. We also omit knowledge of the form drag, which is mostly important in setting the mean flow profile. In the present work, wave correlated laminar velocities are to be constructed from the flow model of Åkervik and Vartdal (2019), with the modification that explicit Reynolds stresses are replaced by an eddy viscosity model.

The model of Åkervik and Vartdal (2019) is a perturbation model, *i.e.* where solutions are sought as perturbations about some reference state. This is a well known technique in stability analysis, and the famous Miles model (Miles, 1957) is based upon the wave response being a perturbation to the mean flow. The model of Åkervik and Vartdal (2019) instead defines the mean flow as perturbations about a wave induced flow field. A nonlinear model is successively built, starting from a wave flow field similar to Harrison (1908); Lamb (1924). Specifically, Åkervik and Vartdal (2019) allow the kinematics of the wave to drive the *laminar flow* solution given by the velocity field $\mathbf{u}_w$ and pressure field p_w which satisfies the Navier-Stokes equations

$$\frac{\partial \mathbf{u}_w}{\partial t} + (\mathbf{u}_w \cdot \nabla)\mathbf{u}_w = -\nabla p_w + (1/Re)\nabla^2 \mathbf{u_w} \quad \text{Interior domain} \tag{3.1}$$

$$\mathbf{u}_w = 0 \quad @ \quad z = h, \tag{3.2}$$

$$\mathbf{u}_w = ack(\sin(k(x-ct)), 0, \cos(k(x-ct))) \quad @ \quad z = \eta(x,t) = a\sin(k(x-ct)). \tag{3.3}$$

This wave driven flow field is allowed to interact with a *turbulent boundary layer* type pressure driven flow. The Reynolds averaged formulation of such a flow is given as

$$\frac{\partial \mathbf{u}_h}{\partial t} + (\mathbf{u}_h \cdot \nabla)\mathbf{u}_h + \underbrace{(\mathbf{u}_h \cdot \nabla)\mathbf{u}_w + (\mathbf{u}_w \cdot \nabla)\mathbf{u}_h}_{\text{forcing from wave driven flow}} = -\nabla p_h + (1/Re)\nabla^2 \mathbf{u_h} - \nabla \cdot \overline{\mathbf{u'} \otimes \mathbf{u'}} + \mathbf{F}, \tag{3.4}$$

$$\frac{\partial u_h}{\partial z} = 0, \text{ and } v_h = w_h = 0, \quad @ \quad z = h, \tag{3.5}$$

$$\mathbf{u}_w = 0 \quad @ \quad z = \eta(x,t). \tag{3.6}$$

[1] Foken (2006) is not the original reference, but the theory is probably best understood from this reference. A translation of the original work of Monin and Obukhov in 1954 is found at `https://gibbs.science/efd/handouts/monin_obukhov_1954.pdf`

The two-dimensional equations (streamwise-vertical) were discretized directly using a two-dimensional collocation method which casts the Navier-Stokes in to a linear algebra matrix vector type of system that could be solved in `Matlab/Octave/Python`. This builds on matrix differentiation, *i.e.* where derivatives can be seen as matrix-vector products. See for instance Weideman and Reddy (2000) for a description of the philosophy behind such solution methods. Due to the use of Fourier collocation in the streamwise direction, it is possible to solve the problem using very few points; typically in the range of 4 to 12 collocation points. From the resulting solution $\mathbf{u}_w + \mathbf{u}_p$, we will use the wave correlated velocities, *i.e.* the Fourier components that are multiples of the underlying wave number associated with the wave length of the propagating wave.

3.2 Turbulence models

Åkervik and Vartdal (2019) showed that their model was able to fully represent the turbulent flow field over waves, but it required an extremely careful representation of the turbulent stresses $\overline{\mathbf{u}' \otimes \mathbf{u}'}$. Specifically, in order to reconstruct the form drag and the mean flow (far from the surface), it was necessary to use the Reynolds stresses from the Large Eddy Simulation results. As a result, their model can not be used as a standalone model.

However, in the current problem we will only use the wave correlated velocities from the model, and not the mean wind and associated form drag. The mean wind will be taken as a log-law Monin-Obukhov relation with Charnocks relation for roughness (Charnock, 1955). In order for the model to appear as a standalone tool, we seek to model the turbulent stresses by means of eddy viscosity closures

$$-\overline{\mathbf{u}' \otimes \mathbf{u}'} = \nu_T (\nabla \mathbf{u} + \nabla \mathbf{u}^T), \tag{3.7}$$

where $\nu_T(\mathbf{x})$ is a spatially dependent eddy viscosity. Eddy viscosity models state that there is a direct representation of the turbulent stresses in terms of the gradient of the flow field. This assumption is often justified in turbulent boundary layers, and forms the backbone of so called k-ϵ models (see for instance Durbin and Reif, 2011, for an in depth explanation of RANS models). However, Belcher and Hunt (1998) identified a so-called Rapid-distortion region in the flow over waves. In such regions, eddy viscosity models are not valid, since instant equilibrium is violated. Åkervik and Vartdal (2019) also demonstrated that this type of models could not be used to fully describe the flow.

In the interest of creating an operational model, we tentatively introduce an eddy viscosity model and test it against LES data. The model is the framework by Cess (1958); Reynolds and Tiederman (1967),

$$\nu_T = \frac{\nu}{2}\left\{1 + \frac{\kappa^2 \mathrm{Re}_\tau^2}{9}(1-\eta^2)^2(1+2\eta^2)^2 \times \{1 - \exp\left(\mathrm{Re}_\tau / A\left(|\eta| - 1\right)\right)\}^2\right\}^{1/2} - \frac{\nu}{2}, \tag{3.8}$$

which has been used in several recent studies (see for instance del Álamo and Jimenez, 2006; Cossu et al., 2009). In this expression, $\eta = z/h$, is the scaled wall distance, κ is the von-Karman constant, and Re_τ is the friction Reynolds numbers. The parameter A as well as the von-Karman constant are tunable, and values of $A = 25.4$ and $\kappa = 0.426$ were used in del Álamo and Jimenez (2006) for

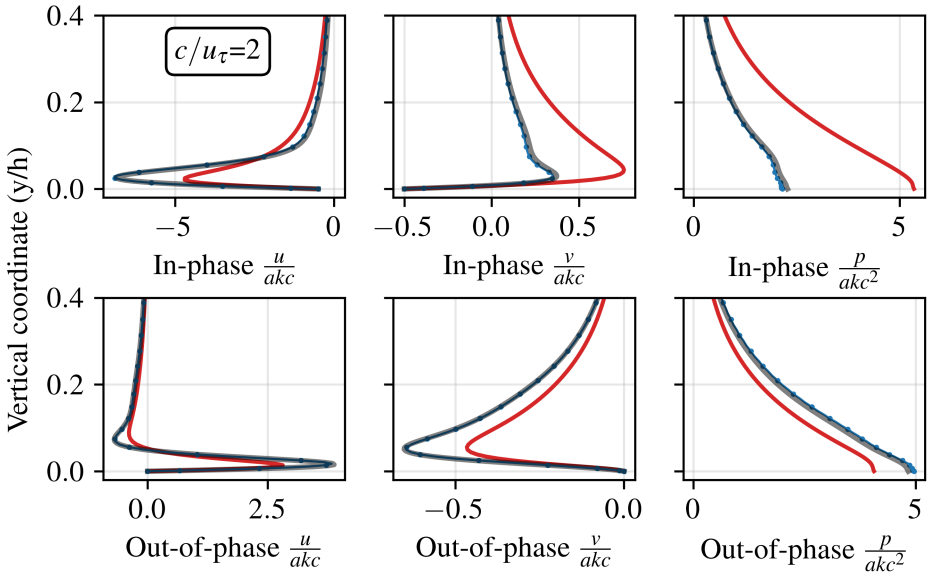

Figure 3.1 *Comparison of simplified model against LES results for a low wave age $c/u_\tau = 2$ and Reynolds number $Re_\tau = 395$. The plot shows in-phase and out-of-phase profiles,* i.e. *the Fourier components with the same wave length as the underlying wave. The gray lines show LES results, the blue lines show the simplified model with Reynolds stresses taken from the LES, and the red lines show the wave model with an eddy-viscosity model. At this low wave age the wave correlated flow is tightly linked to turbulence.*

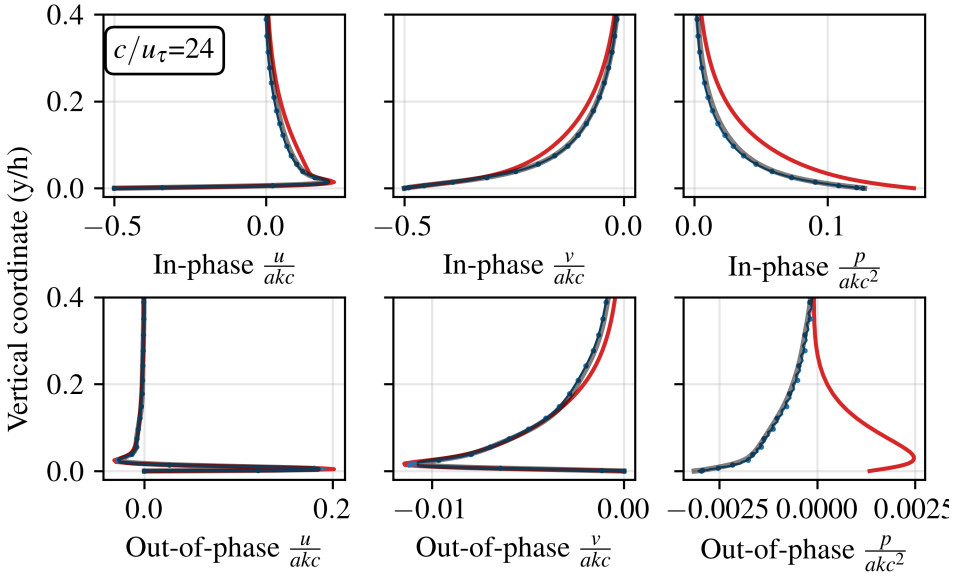

Figure 3.2 *Comparison of simplified model against LES results for a high wave age $c/u_\tau = 24$ and Reynolds number $Re_\tau = 395$. Lines are the same as in fig. 3.1. At this high wave age, the wave correlated flow is well described when using an eddy viscosity model, even though the form drag (out-of-phase pressure) is completely off.*

turbulent channel flow up to $\mathrm{Re}_\tau = 2000$. This eddy viscosity is consistent with a mean flow profile of an open channel, obtained as the integral of

$$\frac{\mathrm{d}U}{\mathrm{d}z} = \frac{u_\tau^2}{h(\nu_T + \nu)}(h - z). \tag{3.9}$$

In figs. 3.1 and 3.2, we compare the wave model with LES results of Åkervik and Vartdal (2019) on a laboratory scale for wind sea and swell sea, respectively. In the figures, we use the wave model with Reynolds stresses taken from the LES, for which the model by construction should match the LES, and the wave model with an eddy-viscosity closure. The key takeaway from the comparison is that an eddy viscosity closure can not describe correctly the pressure. However, wave correlated velocities are well described for the swell case, and reasonably well described for the wind sea case. It therefore appears that the eddy viscosity closed modification of the Åkervik and Vartdal (2019) model is of sufficient quality for use in conjunction with a particle method.

On the atmospheric scale, we skip the complicated eddy viscosity formulation of Cess (1958); Reynolds and Tiederman (1967), and instead use an eddy viscosity that matches the classical Monin-Obukhov log profile, which in derivative form reads

$$\frac{\mathrm{d}U}{\mathrm{d}z} = \frac{u_\tau}{\kappa z}. \tag{3.10}$$

Our aim is to obtain an eddy viscosity profile that simultaneously satisfies a pressure driven formulation and the log profile. To this end, we combine eq. (3.9) and eq. (3.10) to end up with an eddy viscosity

$$\nu_T = \max\left(\frac{\kappa u_\tau}{h} z(h - z) - \nu, 0\right). \tag{3.11}$$

The Monin-Obukhov similarity theory is strictly based on constant stresses throughout the surface layer (Foken, 2006), which is not satisfied for pressure driven flow (Pope, 2000). This may explain why many atmospheric boundary layer studies instead use a shear driven (Couette) formulation (see for instance Sullivan et al., 2000). We are aware of this slight inconsistency, but Åkervik and Vartdal (2019) showed that for the wave correlated velocities the pressure driven and shear driven formulations give more or less identical results. In the future, we could implement our wave model in a shear driven formulation, but since we regard this inconsistency to be of less importance for the current use, we proceed with the pressure driven formulation.

The resulting mean flow profile can be written as

$$U(z) = \frac{u_\tau}{\kappa} \log(z/z_0). \tag{3.12}$$

For the flow over waves, (Peña and Gryning, 2008, fig.7) showed on the basis of offshore observations, that Charnocks relation (Charnock, 1955) was well suited to relate the observed drag from the waves on the wind. Charnocks' relation is given as

$$z_0 = \alpha_c u_\tau^2 / g + 0.11\nu/u_\tau, \tag{3.13}$$

where $\alpha_c = 1.2 \cdot 10^{-2}$ is a tunable constanat, $g = 9.81\mathrm{m/s}^2$ is the gravitational acceleration, and $\nu = 1.5 \cdot 10^{-5}$ m^2/s is the kinematic viscosity of air. The roughness length is the integration constant

in eq. (3.10), and represents the aerodynamic drag provided by the rough surface (Charnock, 1955). The last term is the aerodynamically smooth limit. Compared to onshore surfaces, offshore surfaces are very smooth. At 5 and 15 m/s, eq. (3.13) yield roughness lengths of $4.3 \cdot 10^{-5}$ m and $4.4 \cdot 10^{-4}$ m, respectively. In comparison, grass areas yield aerodynamic roughnesses in the order of 0.5 m, and desert and tundras roughnesses around 10^{-2} m (IFS - Part IV, 2021).

In our wave model, the mean flow is not specified a priori. Instead, it is the result of the integration of an equation similar to eq. (3.9). The specification of the eddy viscosity is hence the driving factor in establishing the mean flow. Close to the surface, the model gives a viscous region, *i.e.* where the mean flow has a linear profile. This is strictly not compatible with the definition of the surface roughness, which is "the height above the surface at which the mean flow is zero". However, the wave model is only sensitive to the mean shear, and this is correctly captured in the model.

4 Quasi-laminar transport by wave motion

We now proceed to the verification of our model. First, consider the pure transport by the shear-flow (*i.e.* mean profile) and the laminar wave response. This is often referred to as a quasi-laminar state (Miles, 1957), since the model is laminar, but the mean flow profile stems from a turbulent state.

Figure 4.1 shows the pathlines for several high inertia particles (as signified by a Stokes number in (see eq. (2.3)) of approximately 1). The starting positions are shown as red dots in the top frame. The top frame shows the flat boundary layer flow, the middle frame shows the wind sea case $c/u_\tau = 2$, and the bottom frame shows the swell sea case $c/u_\tau = 24$.

In the top frame, the mean flow is the only available transport mechanism. The end result is straight pathlines. The wavy surface adds wave correlated motion that affects the transport of particles. For the low wave age case, this results in the trapping of particles close to the surface, and high inertia particles are deposited on the surface. This is seen as black dots in the plot. For the high wave age case in the bottom frame, the wave motion contributes to a net upwards motion of the particles, *i.e.* away from the surface. Deposition only occurs to those particles that originally started very close to the surface during the first passage over a wave, but there is no mechanism present that yields net downwards transport or particles.

The particle transport mechanism due to propagating waves is therefore clear; for wind seas (low wave ages) there is a net downwards motions and particles are deposited on the surface. For swell seas (high wave ages) there is a net upwards mechanism. This was also observed in Åkervik (2022), but here we show the laminar wave mechanism in isolation, without turbulence. The mechanism is valid for all Stokes numbers, but becomes more pronounced with increasing Stokes number. For sufficently large particles however, the response time (inertia) of the the particles becomes so large compared to the wave period, that it can not respond to the wave flow field (see Åkervik, 2022, for a discussion on deposition rate).

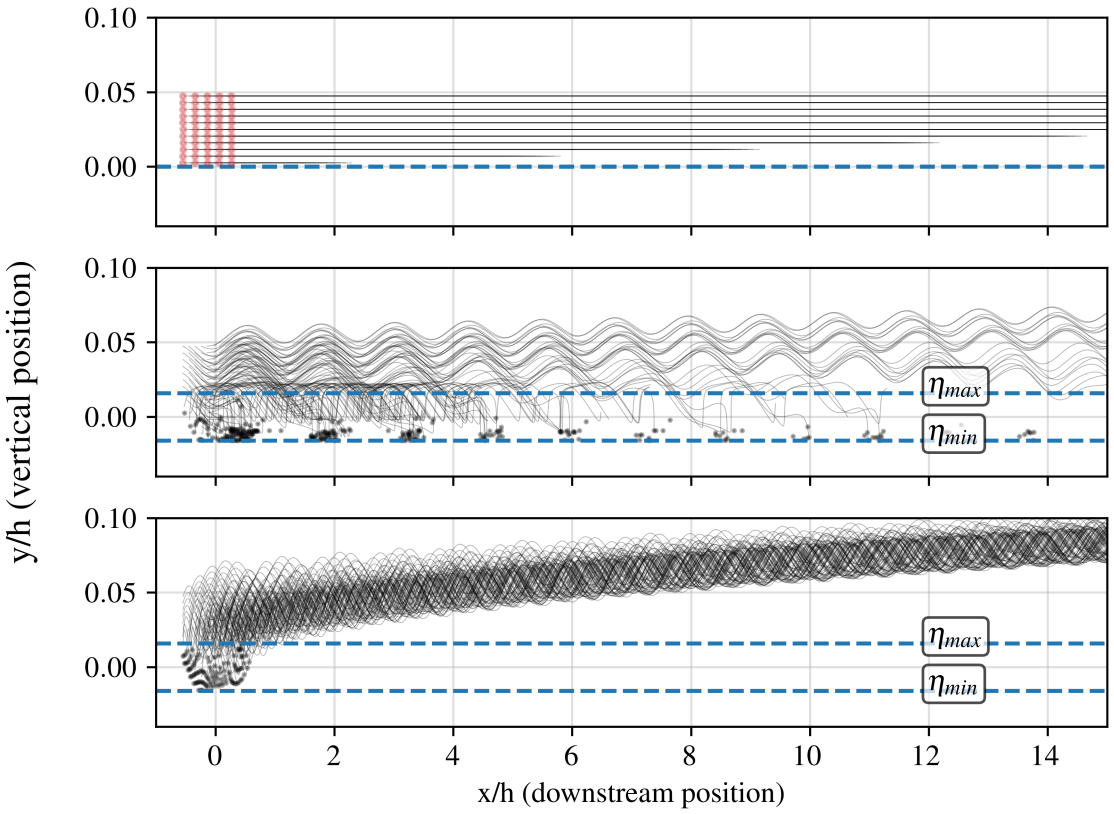

Figure 4.1 *Pathlines of high inertia particles for laminar transport. Top frame shows particle tracelines for flat boundary layer flow, the middle frame shows the low wave age case, and bottom frame shows the high wave age case. The red dots in the top frame signify the initial positions, and the black dots signify deposited particles. Blue dashed lines signify ± the wave amplitude.*

5 Laboratory scale verification

In the previous section, we considered only the transport provided by the laminar wave response. However, the ultimate goal is to combine the effects of laminar wave motion and turbulent motion to end up with a fully functional dispersion model. In this section, we seek to verify our model against the three laboratory scale high fidelity model cases of Åkervik (2022). These are; the flat boundary layer flow, the low wave age case (wind sea), and the high wave age case (swell sea).

5.1 About the results of Åkervik (2022)

Åkervik (2022) studied the particle transport in a two-phase (air-water) system, where the surface was either flat [2], governed by slow waves (wind sea regime), or fast waves (swell sea regime). The surface interaction was described by a so called Volume of Fluid (VOF) method, and the particle transport in the LES was described by eqs. (2.1) to (2.3) and (2.5). The particle tracking was updated during the flow simulation, and turbulent flow fields were therefore available at every time step. There was hence no need for any random walk model to account for turbulence. Note that gravitional pull was turned off in order to elucidate only the flow influence on particle transport. In real situations however, gravitational settling has to be retained.

We compare the high fidelity data in Åkervik (2022) with the data obtained from our random walk model. The random walk model takes the following input: The mean wind profile $\mathbf{U}(\mathbf{x}_p) = (U(z_p), 0, 0)^T$ and the profiles of the turbulent stresses $\sigma_x(z_p)$, $\sigma_y(z_p)$, and $\sigma_z(z_p)$. To calculate the integral time scales, we need the turbulent dissipation rate ϵ. While this type of data is readily

[2]The flat boundary layer flow has some small ripples at the interface, but the roughness length from these are smaller than the viscous length scale.

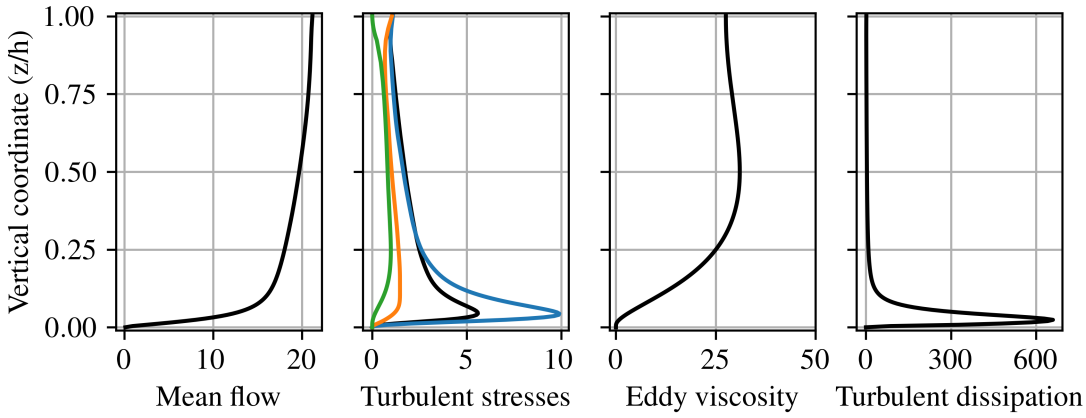

Figure 5.1 Vertical mean profiles of turbulent flow from flat surface LES at laboratory scale. In the second frame from left, the colors signify: Black (turbulent kinetic energy), blue (streamwise Reynolds stress), orange (vertical Reynolds stress), and green (spanwise Reynolds stress).

available from DNS results, most LES studies does not give good estimates. We therefore use the RANS definition of the dissipation (Durbin and Reif, 2011):

$$\epsilon = C_\mu k^2 / \nu_T \,. \tag{5.1}$$

This eddy viscosity can be estimated from the mean flow profiles as $\nu_T = -\langle u'v' \rangle / \frac{\mathrm{d}U}{\mathrm{d}z}$, but here we use the more well-behaved relations given in eq. (3.8). Flow profiles and derived quantities from Åkervik (2022) can be seen in fig. 5.1. We stress that the information provided in the figure is all the information we give the random walk procedure.

5.2 Verification of flat boundary layer passive particles

Our first verification is the particle tracking in the flat boundary layer flow. The particle size is $d_p/h = 10^{-5}$, for which the Stokes number is smaller than 10^{-3}. These particles are hence expected to behave as passive tracers.

The LES has approximately 150000 particles seeded over a vertical cylinder of radius 0.01 in the vertical range of $z/h = -0.2$ to $z/h = 0.4$, but in order to keep the computational cost low, we consider only a subset of 20000 particles seeded in the vertical range of $z/h = 0$ to $z/h = 0.3$. The particle model is initiated with the same 20000 particles and particles are allowed to propagate according to the mean flow and the turbulent stresses.

Figure 5.2 compare concentrations of the random walk with the LES at different times in side views and top views, respectively. Initially, all particles are located in a small region close to $x/h = 0$, and the corresponding concentration is one by construction. As time progresses, particles are transported downstream by the mean flow as they are smeared out by turbulence.

As can be seen from the figure, the random walk model is in very good agreement with the LES. The puff front location appears to be well described by the random walk model at all heights. Also the puff trailing edge close to surface appears to be well described. The main difference between the random walk and the LES is the higher concentration close to the surface in the random walk model. It appears that the random walk model slightly underestimates the vertical transport close to the surface, so that more particles are stuck close to the surface than in the LES. This can be seen from the point clouds in the figure, where black markers show LES particles whereas orange markers show random walk particles. The puff footprint seen in the bottom frames, shows that lateral dispersion of the two are very similar, but the random walk model yields a slightly wider plume in the streamwise direction for late times.

5.3 Transport of larger particles in the wind sea regime

The second verification is the transport of particles over slow waves. Again, we consider 20000 particles seeded in the region $z \in [0,\ 0.3]$, and the Stokes number is slightly larger than 1.

Åkervik (2022) showed that in this flow regime, high Stokes number particles tend to be deposited on the surface. The author proposed that the mechanism that leads to particle deposition is that

particles are thrown down towards the surface by turbulent motion. Small particles then become trapped in the Kelvin's cat's eyes (Thomson, 1880), before turbulence gradually ejected the particles back into the turbulent flow. Larger particles, on the other hand, can not follow the curvature of these fluid pathlines. The result is that these particles crash into the surface. Note that this deposition is not due to gravity, since gravity was not included in the simulations. When included, gravity will increase the level of deposition.

As we could see in fig. 3.1, the wave correlated motion could only partly match the LES when using an eddy viscosity model (which is the model used in the current report). We also know that for such low wave ages, the wave correlated turbulent stresses should be included (Åkervik and Vartdal, 2019). Regardless of this we, attempt to compare the particle transport of our simple model with the LES results.

Figure 5.3 shows a comparison of the time evolution of concentration. The random walk results are again in good agreement with the LES results. As seen from the side view in the top frames, the puff front locations is in excellent agreement with the LES, but the LES has higher concentrations in the outer part of the domain ($z/h > 0.1$) behind the puff center. This tendency is more pronounced than for the flat boundary layer with passsive particles. As for the passive particles over a flat surface, the puff footprint (as seen from above) is in good agreement with the LES in the lateral direction, but the streamwise dispersion is too wide, especially at late times. Since these tendencies are seen both in the flat case and the wavy case, it is likely that the discrepancy is due to the simplistic description of turbulence given by the random walk method.

The LES predicts that at t=1.5, approximately 30 % of the particles has deposited at the surface. The random walk model predicts that approximately 20 % deposit. We therefore end up with slightly higher air concentrations in the random walk model than in the LES. To accurately describe the deposition is probably a difficult task, but the current results may be seen as a good agreement. Some possible explanations to the discrepancy may be: i) The wave correlated laminar motion is underestimated by our model. ii) The wave correlated turbulent stresses are neglected in the model. iii) The random walk turbulence is not accurate enough (no off diagonal stresses, and simple time scale model) to capture the delicate interaction between turbulence and wave correlated motion. Since we for the laboratory scale have access to Reynolds stresses from the LES, we could skip the use of eddy viscosity model in our wave description. This leads to wave correlated laminar flow fields in close agreement with the LES. However, this did not affect the results significantly; deposition remains slightly underestimated. Therefore, the underestimation appears to stems from the less precise description of turbulence in the random walk model.

This section is first and foremost a proof of concept that the model can describe the downwards transport of particles present in an idealized unimodal version of wind seas. A real wind sea regime has a multimodal character, where several waves of different wave length and propagation direction interact to form complex surface patterns. It could in principle be possible to compute the wave flow profiles from each of these different wave components and superpose them. This is an interesting topic, but outside of the scope of the current work. A wave age of $c/u_\tau \approx 2$ corresponds to wave lengths smaller than 1 m, which is small compared to a 100 m thick boundary layer. It is therefore possible that the flow response to such waves may equally well be described as a "roughness" with no specific treatment of the wave response (as assumed in Li et al., 2019, and others).

5.4 Transport of larger particles in the swell wave regime

The third verification is the transport of particles in the swell wave regime. As in the previous section, we seed 20000 particles at heights between 0 and 0.3 with Stokes number slightly above 1, *i.e.* particles with high inertia.

For this configuration, Åkervik (2022) showed that there was an effective transport mechanism away from the surface for larger particles. In this case, particles that are thrown down to the surface by turbulence will meet an upwards mechanism, as seen in fig. 4.1.

In this case, the eddy viscosity model lead to wave correlated laminar velocities in close agreement with LES. We therefore expect our model to perform better than for wind seas.

Figure 5.4 shows a comparison of the time evolution of concentration. Our model is able to capture the increased outwards transport by the swell waves, as seen by the fact that the puff moves, in close agreement with the LES results, more as an isolated blob than for the flat case and the wind seas. Again the puff front location is in good agreement with the LES, and the surface footprint is in excellent agreement. However, as seen from the side view in the top frames, also here there is lower concentration in the outer domain compared to the LES.

5.5 Summary of laboratory scale comparison

The key takeaways from the comparison with high fidelity data are:

- The random walk model yields turbulent diffusion in good agreement with LES data. The puff front location, and the lateral dispersion is in excellent agreement with the LES. However, the random walk model yields slightly higher concentrations close to the surface, and therefore leads to slightly shorter puff extent in the streamwise direction far from the surface.
- The influence of waves is well described both for the wind sea and the swell sea regime, *i.e.* for both slow and fast waves compared to the mean wind. In the wind sea example, the model is to some degree able to describe the deposition caused by the trapping of particles in the Kelvin's cat's eyes, *i.e.* the simple model captures two thirds of the deposition rate in the LES. For the swell sea case, the model is able to describe the added upwards transport provided by the waves, and the LES and random walk model both predict that the puff is transported downstream as an isolated blob, contrary to the flat surface case and the slow wave case, where many particles are trapped close to the surface.

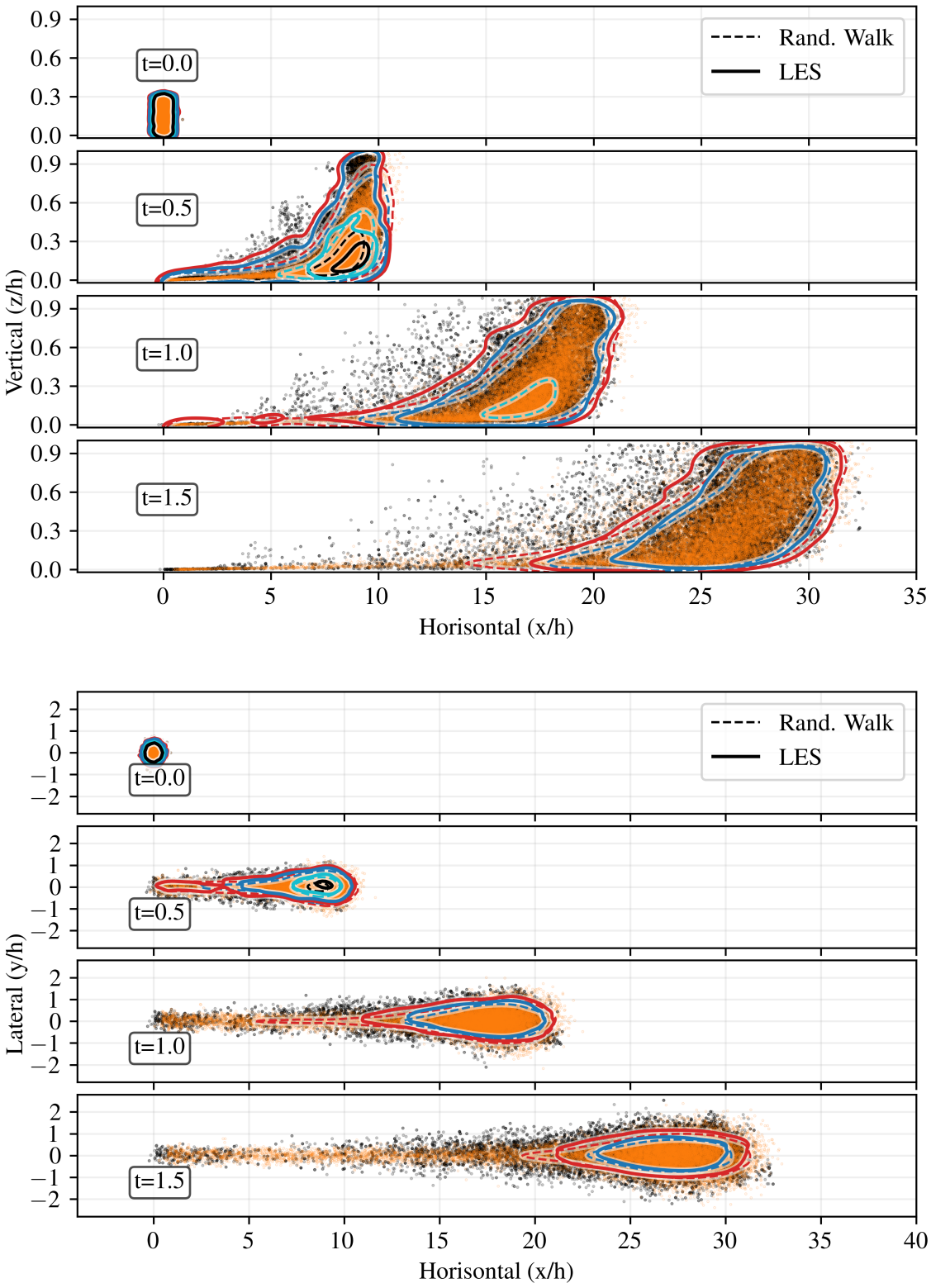

Figure 5.2 Flat boundary layer flow with low inertia/passive particles. Density contours calculated from point clouds from LES (solid lines) and the random walk model (dashed lines). LES and random walk point clouds are shown as black and orange markers, respectively. The different contours show concentrations 10^{-1} (black), $5 \cdot 10^{-2}$ (cyan), 10^{-2} (blue), and $5 \cdot 10^{-3}$ (red).

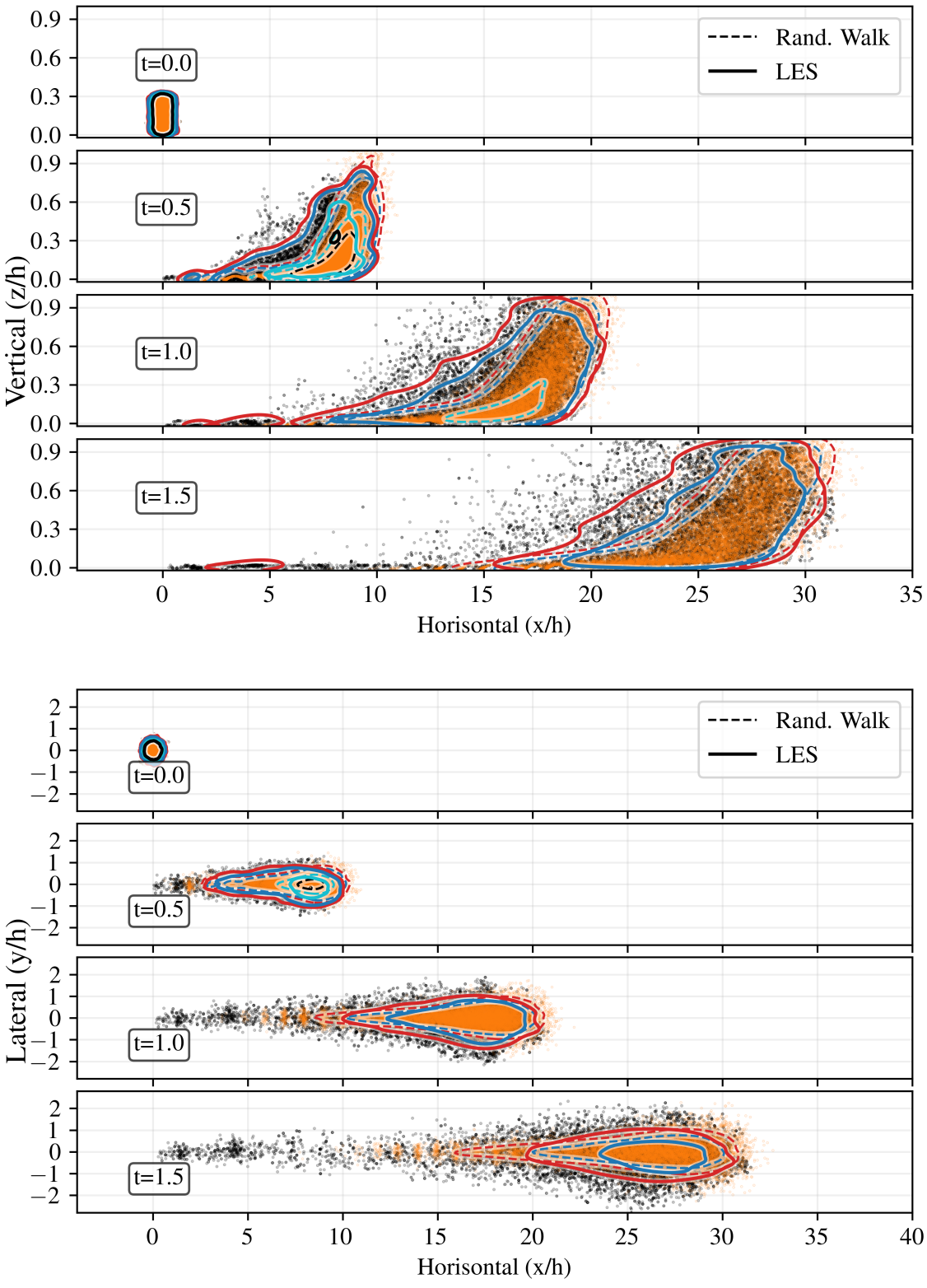

Figure 5.3 *Low wave age flow with high inertia particles. Density contours calculated from point clouds from LES (solid lines) and the random walk model (dashed lines). LES and random walk point clouds are shown as black and orange markers, respectively. The different contours show concentrations 10^{-1} (black), $5 \cdot 10^{-2}$ (cyan), 10^{-2} (blue), and $5 \cdot 10^{-3}$ (red).*

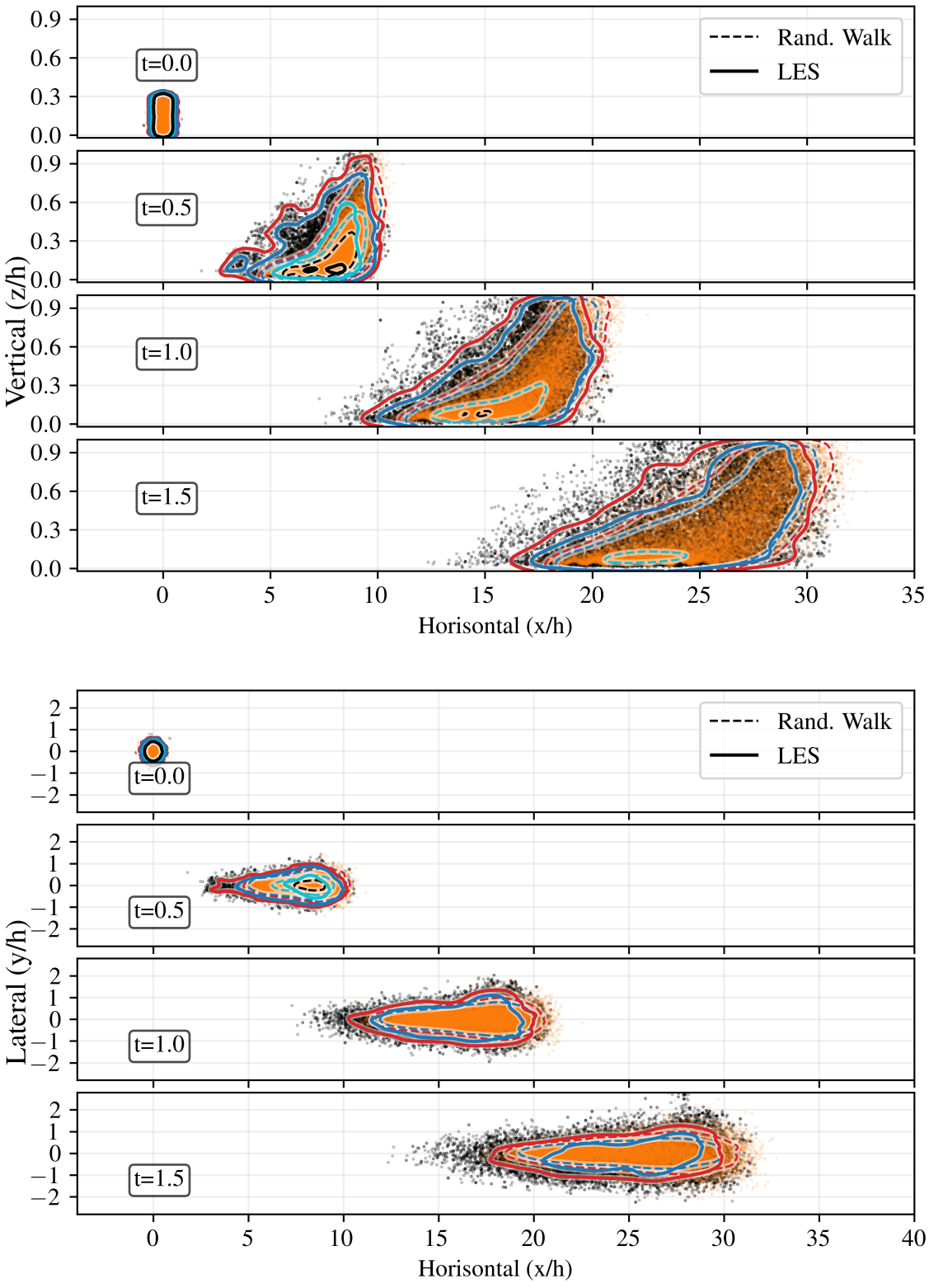

Figure 5.4 High wave age flow with high inertia particles. Density contours calculated from point clouds from LES (solid lines) and the random walk model (dashed lines). LES and random walk point clouds are shown as black and orange markers, respectively. The different contours show concentrations 10^{-1} (black), $5 \cdot 10^{-2}$ (cyan), 10^{-2} (blue), and $5 \cdot 10^{-3}$ (red).

6 Extension to operational scale

In this section we perform tests to assess the usefulness of our model on an operational scale. In the previous sections, we compared our dispersion model to high fidelity LES data on very small scales. One of the idealizations we did on the lab scale, was to turn off the gravitational pull on particles and to tune how the gravitational acceleration affects the waves (Froude number) in order to achieve different sea states at the same wave length. On the operational scale we need to retain gravitational pull. Furthermore, the wave speed (c) is determined by the wavelength (λ), such that $c = \sqrt{(2\pi)^{-1} g\lambda}$, where $g = 9.81\,\mathrm{m/s^2}$ is the gravitational acceleration. Hence, if we consider a flow with friction velocity of $u_\tau = 0.4\,\mathrm{m/s}$, a typical wind-sea wave-age of $c/u_\tau = 2$ can be achived for the wavelength of $\lambda = 0.4\,\mathrm{m}$, which is very short compared to a typical boundary layer height of approximately 100 m. Similarly, a typical swell-sea wave-age of $c/u_\tau = 30$ can be achieved for wavelengths of approximately $\lambda = 100\,\mathrm{m}$, which is comparable to the boundary layer height. Hence, swell waves influence the flow on a much larger scale than wind waves. Gravitational pull has a profound influence on the dispersion pattern. The gravitational pull leads to a settling velocity which represents the balance of buoyant forces and drag forces, as seen in eq. (2.2). A water particle of size 1 μm suspended in air has a negligible settling velocity on the order of $10^{-5}\,\mathrm{m/s}$, whereas a particle of size 100 μm has a settling velocity on the order of $10^{-1}\,\mathrm{m/s}$ which is comparable to the flow velocities, and a particle will hence descend on the order of ten meters every minute.

Operational scales can range from meters to several hundreds and thousands of kilometers. Here we consider dispersion within some kilometers, since this is sufficient to elucidate the effects of waves. We consider the case where wind and waves are aligned, although swell waves can in principle propagate in any direction (Semedo et al., 2011). On the operational scale we do not have access to high-fidelity wind data. Therefore, mean flow profiles will be taken as simple analytical profiles. Central to such profiles is the concept of surface roughness. Over land, surface roughness is tightly coupled with the geometric features of the surface Foken (2006). However, over seas, the roughness is meant to account for short wind waves, and this is often taken as the Charnocks roughness length (Charnock, 1955).

As in Li et al. (2019), we follow this strategy and use the surface roughness to model the influence of wind seas. Hence, we do not attempt to model the trapping of particles close to the surface as we did on the laboratory scale. This is not to say that this effect is not present of large scales, but we expect that a spectrum of these short and slow waves will compete to create complex flow patterns that are probably best described as a "roughness". Note that also swell seas are subject to multimodal behaviour (Semedo et al., 2011, 2015), with shorter waves riding on top of longer waves. In the present work we use the idealization that we have one swell wave propagating in the direction of the flow, with shorter waves riding on top of them. We hence resolve the swell wave, but model the shorter waves as a roughness length.

In our operational-scale test case, we consider a $h = 100$ m deep boundary layer with a mean wind speed at $z = 10$ m of $U_{10} = 10$ m/s. The Charnocks relation (eq. (3.13)) then gives a roughness length of $z_0 = 1.8 \cdot 10^{-4}$ m and a friction velocity of $u_\tau = 0.37$ m/s. This specific case is chosen to match the LES results of Li et al. (2019). We will compare our flat surface wind sea (*i.e.* a roughness profile to account for short waves) results with a Gaussian puff model, and the swell wave case with Li et al. (2019).

The analytical vertical mean flow (and turbulence) profiles used in our operational test cases is

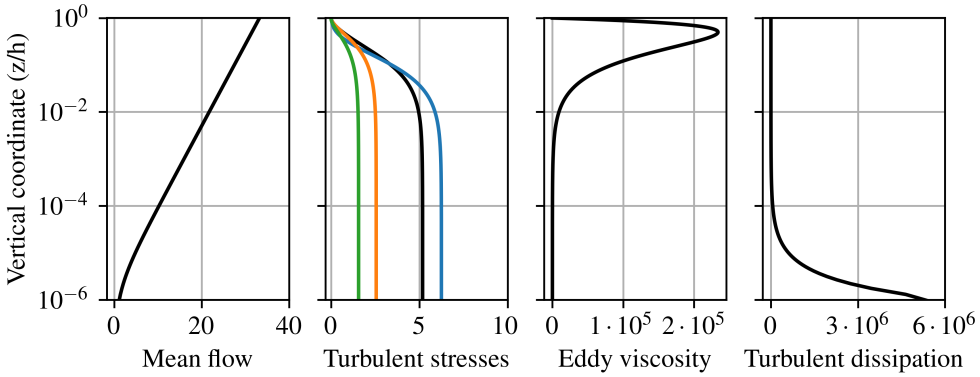

Figure 6.1 Analytic atmospheric boundary layer profiles. From left to right we show the mean flow profile, the turbulent stresses, the eddy viscosity and the turbulent dissipation. In the second frame from left, the colors signify: Black (turbulent kinetic energy), blue (streamwise Reynolds stress), orange (vertical Reynolds stress), and green (spanwise Reynolds stress).

shown in fig. 6.1. In the figure, the vertical coordinate is on a log scale, which leads to a linear mean wind profile. The turbulent stresses are taken from Stull (2015), the eddy viscosity model is the one proposed in eq. (3.11), and the turbulent dissipation is given in eq. (5.1). The mean flow profile will transport particles downstream in a steady fashion, whereas the turbulent stresses will contribute to turbulent diffusion of the particles through the random walk method. The eddy viscosity will be used both in the wave model and in the estimation of time scales for the random walk.

6.1 Wind sea roughness boundary layer, comparison with Gaussian models

First, consider the transport over a flat roughness dominated surface, where the roughness is meant to account for short waves, or the early stages of wind seas (Sullivan et al., 2014; Yang et al., 2013a).

We seed 20000 particles of size 10μm and density $\rho_p = 1000\,\mathrm{kg/m^3}$, for which the Stokes number is smaller than 10^{-1} in most of the domain and the settling velocity is only 3 mm/s. In this case, it is natural to compare the result with a Gaussian model (Hanna et al., 1977). Since we here consider instantaneous releases, the relevant form are those of Gaussian *puff* models. We here use the form given in the RIMPUFF description (Thykier-Nielsen et al., 1999):

$$c(x,y,z,t) = \frac{Q}{(2\pi)^{3/2}\sigma_{xy}^2\sigma_z}\exp\left(-\frac{1}{2}\frac{(x-Ut)^2+y^2}{\sigma_{xy}^2}\right)\times \left(\exp\left(-\frac{1}{2}\frac{(z-H)^2}{\sigma_z^2}\right)+\exp\left(-\frac{1}{2}\frac{(z+H)^2}{\sigma_z^2}\right)\right), \quad (6.1)$$

where x is the streamwise direction (along the mean wind U), y the lateral direction and z the vertical direction. H is the location of the source in the vertical direction, and t is time. We use the dispersion parameters from the ALOHA® technical description (Jones et al., 2013). In the

Table 6.1 Dispersion parameters for neutral conditions as defined in Jones et al. (2013).

Stability class	$a_{x,y}$	$b_{x,y}$	a_z	b_z	c_z
D (neutral)	$8 \cdot 10^{-2}$	$1 \cdot 10^{-4}$	$6 \cdot 10^{-2}$	$1.5 \cdot 10^{-3}$	-0.5

technical description they hint towards the use of a low roughness for offshore conditions, but it is unclear how they use the resulting mean wind profile. We interpreted the description so as to use the same height dependent Monin-Obukhov profile as we use in our particle model. In Jones et al. (2013), they use the dispersion parameters developed by Briggs (1973) which is a function of the downstream distance and the Pasquill-Gifford-Turner stability classes. In that framework, the roughness is either "high" (urban, forested, ...) or "low" (rural, grasslands, offshore, ...). We choose a low roughness and neutral stability conditions (class D) for our comparison. The equations for the dispersion parameters are then [3]

$$\sigma_{x,y} = \frac{a_{x,y}x}{1 + b_{x,y}x} \quad \text{and} \quad \sigma_z = a_z x(1 + b_z x)^{c_z}, \tag{6.2}$$

where the parameters are given as in table 6.1.

Figure 6.2 shows a comparison between our particle method (dashed lines) and the Gaussian puff model (solid lines) within the first four minutes after a release. The agreement between the two is generally good, although it appears that the Gaussian puff model smears the concentrations more than the particle model. This is especially evident in the transverse direction. In the Gaussian model, the center of mass appears to be lifted away from the surface, as seen in the wider vertical profile in the right frame. It may be that one could be more specific in how one chooses the dispersion parameters in the Gaussian model, but the parameters chosen here is representative of how one would use a Gaussian model. One positive aspect, is that the two models yield approximately the same puff center location in the streamwise-lateral direction. It would be interesting to investigate the discrepancies in more detail, but this would require the use of high fidelity wall modeled LES, which is outside the scope of the current report. If our model is correct, then a Gaussian model would yield far too wide dispersion patterns.

6.2 Swell wave boundary layer

In Li et al. (2019), the authors considered the dispersion of oil droplets from a near surface spill in the presence of 100 m swell waves. The authors use an Eulerian method[4] to compute air concentrations for particle sizes 2.5, 40, 60 and 100 μm. For the largest particle size, the authors showed, through concentration contours, that deposition due to gravitational pull was substantial. In all cases, they demonstrated that swell waves lead to an effective "pumping" of the aerosols away from the surface. They attributed this to the altered vertical turbulent fluctuations. Compared to a roughness

[3]Jones et al. (2013) defines separate σ_x and σ_y, but their description of σ_x is confusing. We therefore set $\sigma_{x,y} := \sigma_x = \sigma_y$ in line with Thykier-Nielsen et al. (1999).

[4]They solve an advection-diffusion equation alongside the Navier-Stokes equations, (see for instance Åkervik and Gjesdal, 2023)

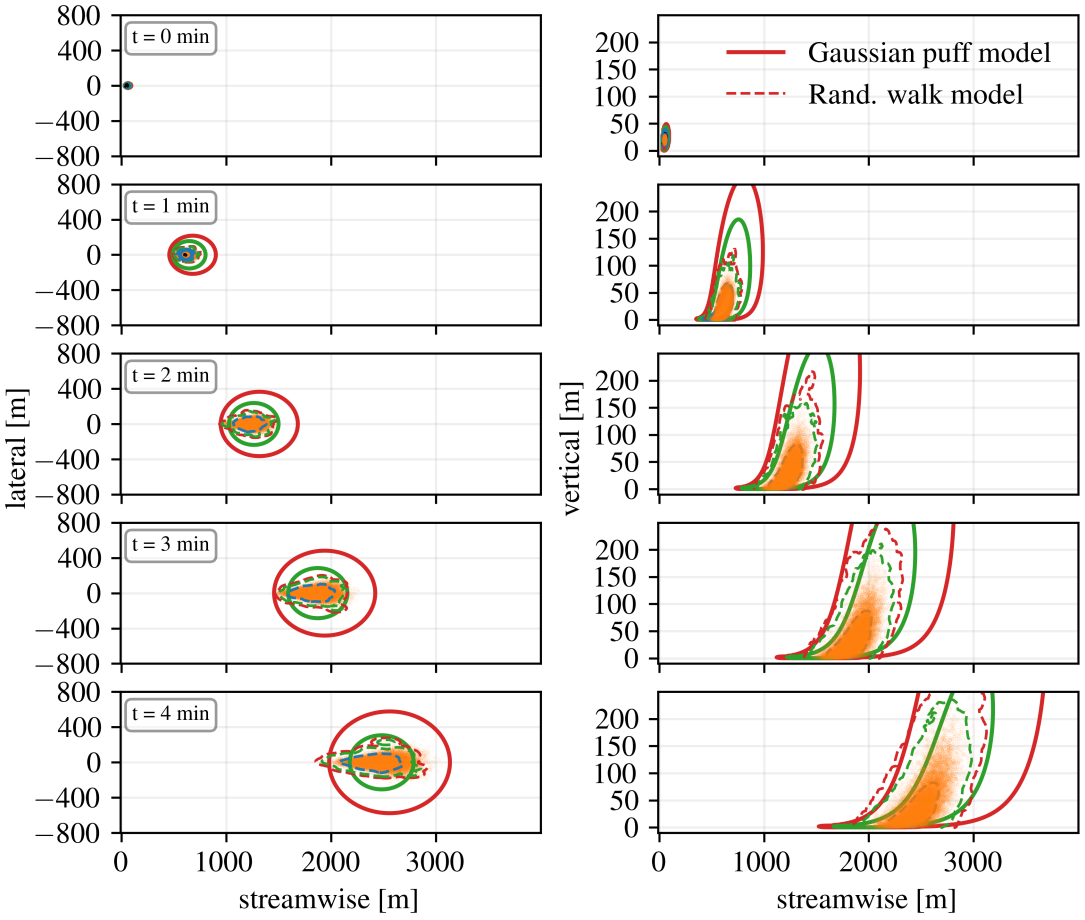

Figure 6.2 *Comparison of concentration contours from particle model and particle size d_p = 10 μm (dashed lines) and a Gaussian puff solution with dispersion parameters taken from ALOHA (solid thick lines). The different contours show concentrations 10^{-1} (black), 10^{-3} (blue), 10^{-5} (green), and 10^{-7} (red). The orange dots show particles.*

dominated wind-sea state, the resulting center of mass of the aerosols moved approximately 2 meters further out from the surface 600 meters downstream. The method used by Li et al. (2019) is an advanced surface modelled LES that requires substantial computational resources and time to solve.

Our wave model is built around laminar wave correlated velocities, and does not contain the altered *turbulent* fluctuations due to the swell wave. The wind wave interaction problem is very delicate and difficult to understand, and turbulence is an integral part of the system. For wind seas, wave correlated turbulent stresses dictate the wave correlated laminar response (Belcher and Hunt, 1998; Åkervik and Vartdal, 2019). For swell seas, wave correlated turbulence is still present, but the wave correlated laminar response is first and foremost governed by the wave kinematics, as explained by Åkervik and Vartdal (2019). We seek to test if the behavior in Li et al. (2019) can be explained by these laminar mechanisms. If it can not, then our model is not very useful, and we can discard it. However, if we can explain the same type of behavior, then the conclusion of Li et al. (2019) may

have to be revised, and our model may hold value for offshore dispersion of aerosols.

We consider the swell wave regime, with long waves that propagate beneath the boundary layer. We consider two cases; one with wave length $\lambda = 100$ m, and one with wave length $\lambda = 200$ m. For reference, we also consider one with a flat bottom (which represents a wind sea state), The flat case and the $\lambda = 100$ m case were also covered in Li et al. (2019). In both wave cases we have wave steepnesses of $ak = 0.1$, so that the $\lambda = 100$ m case has an amplitude of $a = 1.6$ m, and the $\lambda = 200$ m case has an amplitude of $a = 3.2$ m. The corresponding phase speeds are $c = 12.5$ m/s and $c = 17.7$ m/s, respectively. The wave ages based on the friction velocity are hence $c/u_\tau = 34$ and 38 for the two cases. In all cases we seed 10000 particles of size 40μm and density $\rho_p = 850\,\mathrm{kg/m^3}$. The corresponding Stokes number based on the mean flow time scale, ranges from 0.001 to 0.5 in most of the flow domain (above 2 cm from the surface), and the settling velocity is 5 cm/s. The flat bottom "wind sea" case in this section differs from the one in the previous section by the particle definition, *i.e.* with four times as big diameter and slightly less dense. Note that we have performed test over a wide range of particle sizes, but it appeared that 40μm gave the most interesting results, in that it has some inertia without being completely dominated by gravitational pull.

Figure 6.3 shows a side view of the particle point cloud snapshots during the first minute for all three cases. The mass center is initially located at $x = 0$ m, $z = 1$ m.

For the flat wind sea case, the mass center is located at $x = 540$ m and $z = 8.8$ m after $t = 60$ s, and almost 60 % of the particles have deposited on the surface due to gravitational settling. At the same time, the deposition in the $\lambda = 200$ case is less than 30%, and the mass center is found at $z = 13.1$ m, which is 4.3 m higher than the flat case. For the $\lambda = 100$ m case, the deposition is slightly higher than the $\lambda = 200$ m case, and the mass center at $t = 60$ s is slightly lower, at $z = 10.3$ m. It is evident that deposition is counteracted by the presence of the swell waves. This ultimately leads to higher air concentrations when swell waves are present.

If we compare these results to the work of Li et al. (2019), where they use a continuous ground based source, we find for the flat "wind sea" case, that over a distance of $x = 600$ m our center of mass has lifted 8.5 m, whereas Li et al. (2019) has a lift of slightly less than 8 m. The two results are hence quite similar. Our $\lambda = 100$ m case has a center-of-mass lift of 9.8 m, whereas Li et al. has a lift between 10 m and 11 m, depending on the phase of the wave. In other words, our results show an increase in center-of-mass height of 1.3 m, whereas Li et al. show an increase of approximately 2-3 m. Without specific knowledge of the rate of deposition or concentration in Li et al. (2019) it is difficult to assess the difference. Notice that our $\lambda = 200$ m has an increase in lift between 1 m and 5 m, depending on the phase (see fig. 6.3 bottom frame). Although our model only contains laminar wave correlated stresses, it is able to prevent deposition of particles and lift the particle cloud away from the surface, much in the same way as the state-of-the-art wall modeled LES of Li et al. (2019). It therefore appears that part of the mechanism related to vertical pumping from swell waves is governed by the laminar response to waves, and not turbulence, in contrast to Li et al. (2019).

As in Li et al. (2019), we find that particle sizes of 100 μm and upwards are subject to severe deposition. In our simulations, almost all the 100μm particles of have deposited after one minute. It thus appears that for aerosols of sizes exceeding $100\,\mu$m there is no need for a dispersion model. Our wave model may be therefore be useful for the dispersion of aerosols smaller than roughly 100μm.

The model we have proposed in this work has the major advantage of being computationally efficient. The model can be used to simulate dispersion at operational scale in a few minutes on a standard

laptop, whereas the LES approach of Li et al. (2019) probably requires several days of computation on hundreds of cpu cores.

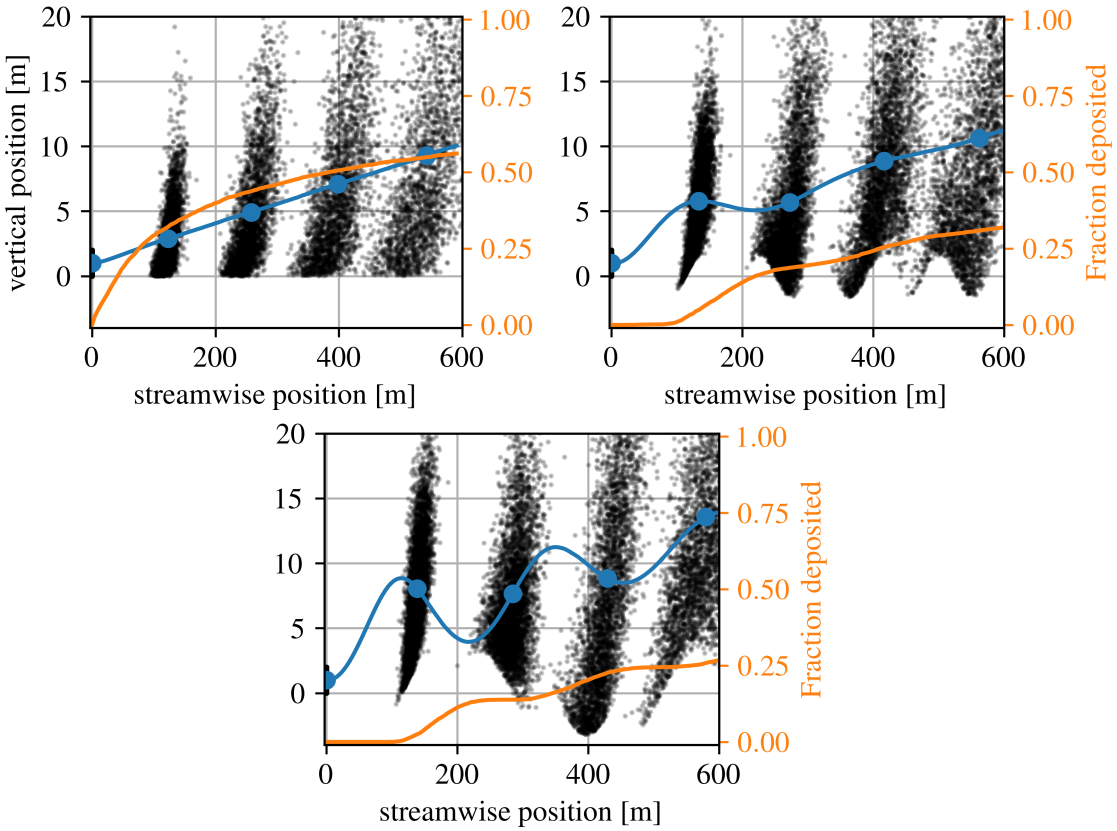

Figure 6.3 *Flat boundary layer (top left), 100 m swell wave boundary layer case (top right), and 200 m swell wave boundary layer case (bottom). Black clouds show* $40\mu m$ *particle positions at times* $t = \{0, 15, 30, 45, 60\}$ *s. The blue dotted lines show the mass center positions, and the orange lines show the fraction of deposited particles.*

7 Concluding remarks

In this report, we have developed a particle based contaminant transport model intended for use on operational scales (meters to kilometers) offshore. Specifically, the model may be useful to account for the added vertical transport provided by swell waves. The novel element in the model is that the effect of waves is described by an easy-to-solve linear algebra type of problem instead of a more complex computational fluid dynamics model.

Offshore verification data on operational scales is difficult to obtain. We therefore verified our model on a laboratory scale. We already knew from previous work that the model would work if we provided enough turbulence information. However, we needed the model to work with as little turbulence information as possible. More specifically, we sought to verify that the use of simple eddy viscosity closures would be sufficient to describe the wave correlated velocities. These are exactly the velocities needed for our particle transport model. Indeed, we could show that on a laboratory scale, the wave correlated velocities were well described using simple turbulence models. Although our results showed that dispersion model does reasonably well in describing the wind-wave regime, we expect our model to be of most value in the swell regime. There are several reasons for this. First, wind waves are very short compared to swell waves, and therefore the velocities generated by the waves do not penetrate as deep into the boundary layer. Whereas wind seas consist of a multitude of waves of different lengths and speeds, it is more likely that swell seas consist of one long wave with short waves riding on top of it. Wind seas may therefore be seen as a flat boundary layer flow with roughness stemming from the waves. On the other hand, swell waves can not be seen as roughness elements and need explicit treatment.

The particle model with a flat lower boundary, reminiscent of the flow over wind-seas, was tested on operational scales against a so-called Gaussian puff model. Gaussian models are the industry standard models, and forms the backbone of the National Oceanic and Atmospheric Administration (NOAA) model ALOHA as well as the danish ARGOS software suite through the so called RIMPUFF model. We show that our particle model yields results that compare reasonably well with a standard Gaussian model. The most significant difference is that the Gaussian model yields a wider plume in the lateral direction and a slightly lifted plume in the vertical direction.

To test the applicability of our model for swell waves, we compare our model with a recently published study on transport of oil spill over swell waves. The oil spill study uses a complex model with time-consuming simulations to show that swell waves lead to increased vertical transport away from the surface. Since finite sized particles are subject to gravitational pull towards the surface, swell waves hence counteracts deposition. Our model can indeed capture this type of phenomenom, and we could show that a 100-meter swell wave propagating under the point cloud of medium-sized particles leads to a factor two reduction in deposition, and therefore also a doubling of air concentration. Our model compares reasonably well to the high-fidelity study on oil spill.

References

Åkervik, E. Aerosol transport in idealized wind-wave systems. Tech. Rep. 22/02547, FFI - Norwegian Defence Research Establishment, 2022. https://www.ffi.no/en/publications-archive/aerosol-transport-in-idealized-wind-wave-systems.

Åkervik, E. and Gjesdal, T. Literature review of atmospheric contaminant transport offshore. Tech. Rep. 23/01769, FFI - Norwegian Defence Research Establishment, 2023. https://www.ffi.no/en/publications-archive/literature-review-of-atmospheric-contaminant-transport-offshore.

Åkervik, E. and Vartdal, M. The role of wave kinematics in turbulent flow over w aves. *J. Fluid Mech*, 880:890–915, 2019. https://doi.org/10.1017/jfm.2019.708.

Belcher, S. E. and Hunt, J. C. R. Turbulent flows over hills and w aves. *Annu. Rev. Fluid Mech*, 30:507–38, 1998. https://doi.org/10.1146/annurev.fluid.30.1.507.

Bocksell, T. L. and Loth, E. Random walk models for particle diffusion in free-shear flows. *AIAA journal*, 39 (6):1086–1096, 2001. https://doi.org/10.2514/2.1421.

Bocksell, T. L. and Loth, E. Stochastic Modeling of Particle Diffusion in a Turbulent Boundary Øayer. *Int. J. Multiphase flow*, 32 (10-11):1234–1253, 2006.

Briggs, G. A. Diffusion estimation for small emissions. *Atmospheric turbulence and diffusion laboratory*, 965:83–145, 1973.

Cess, R. A survey of the literature on heat transfer in turbulent tube flow. *Res. Rep*, pp. 8–0529, 1958. https://www.osti.gov/servlets/purl/4765983.

Charnock, H. Wind stress on a water surface. *Quarterly Journal of the Royal Meteorological Society*, 81 (350):639–640, 1955. https://doi.org/10.1002/qj.49708135027.

Cossu, C., Pujals, G., and Depardon, S. Optimal transient growth and very large–scale structures in turbulent boundary layers. *J. Fluid Mech*, 619:79–94, 2009.

Deskos, G., Lee, J. C., Draxl, C., and Sprague, M. A. Review of wind–wave coupling models for large-eddy simulation of the marine atmospheric boundary layer. *Journal of the Atmospheric Sciences*, 78 (10):3025–3045, 2021. https://doi.org/10.1175/JAS-D-21-0003.1.

Durbin, P. A. and Reif, B. P. *Statistical theory and modeling for turbulent flows* (John Wiley & Sons, 2011).

Foken, T. 50 Years of the Monin-Obukhov Similarity Theory. *Bound. Lay. Met.*, 119:431–447, 2006. https://doi.org/10.1007/s10546-006-9048-6.

Hanna, S., Briggs, G., Deardorff, J., Egan, B., Gifford, F., and Pasquill, F. AMS workshop on stability classification schemes and sigma curves—summary of recommendations. *Bulletin of the American Meteorological Society*, pp. 1305–1309, 1977. https://www.jstor.org/ stable/26218024.

Harrison, W. J. The influence of viscosity on the oscillations of superposed fl uids. *"Proc. Roy. Soc. Lond. Ser. A"*, 2 (1):396–405, 1908. https://doi.org/10.1112/plms/s2-6.1.396.

Hussain, A. K. M. F. and Reynolds, W. C. The mechanics of an organized wave in turbulent shear flow. *J. Fluid Mech*, 41:241–258, 1970. https://doi.org/10.1017/S0022112070000605.

Hussain, A. K. M. F. and Reynolds, W. C. The mechanics of an organized wave in turbulent shear flow. part 3. theoretical models and comparsion with experiments. *J. Fluid Mech*, 54:263–288, 1972. https://doi.org/10.1017/S0022112072000679.

IFS - Part IV, 2021. IFS Documentation CY47R3 - Part IV: Physical processes. 2021. https://doi.org/10.21957/eyrpir4vj.

Jones, R., Lehr, W., Simecek-Beatty, D., and Reynolds, R. M. ALOHA (Areal Locations of Hazardous Atmospheres) 5.4.4: Technical Documentation. Tech. Rep. NOS OR&R 43, U. S. Dept. of Commerce, Seattle, WA: Emergency Response Division, NOAA, 2013. https://response.restoration.noaa.gov/sites/default/files/ALOHA_Tech_Doc.pdf.

Lamb, H. *Hydrodynamics* (University Press, 1924).

Li, M., Zhao, Z., Pandya, Y., Iungo, G. V., and Yang, D. Large-eddy simulations of oil droplet aerosol transport in the marine atmospheric boundary layer. *Atmosphere*, 10 (8):459, 2019. https://doi.org/10.3390/atmos10080459.

Miles, J. W. On The Generation of Surface Waves By Shear Flows. *J. Fluid Mech*, 3:185–204,1957. https://doi.org/10.1017/S0022112057000567.

Peña, A. and Gryning, S.-E. Charnock's roughness length model and non-dimensional wind profiles over the sea. *Bound. Lay. Met.*, 128:191–203, 2008. https://doi.org/10.1007/s10546-008-9323-9.

Pope, S. B. Lagrangian PDF Methods for Turbulent Flows. *Annu. Rev. Fluid Mech*, 26 (1):23–63, 1994. https://doi.org/10.1146/annurev.fl.26.010194.000323.

Pope, S. B. *Turbulent flows* (Cambridge university press, 2000). https://doi.org/10.1017/CBO9780511840531.

Reynolds, W. and Tiederman, W. Stability of turbulent channel flow, with application to Malkus's theory. *Journal of Fluid Mechanics*, 27 (2):253–272, 1967. https://doi.org/10.1017/S0022112067000308.

Schwarzkopf, J. D., Sommerfeld, M., Crowe, C. T., and Tsuji, Y. *Multiphase flows with droplets and particles* (CRC press, Taylor & Francis Group, Boca Raton, Florida, U.S., 2012). https: // doi.org/10.1201/b11103.

Semedo, A., Sušelj, K., Rutgersson, A., and Sterl, A. A global view on the wind sea and swell climate and variability from ERA-40. *Journal of Climate*, 24 (5):1461–1479, 2011. https://doi.org/10.1175/2010JCLI3718.1.

Semedo, A., Vettor, R., Breivik, Ø., Sterl, A., Reistad, M., Soares, C. G., and Lima, D. The wind sea and swell waves climate in the nordic seas. *Ocean dynamics*, 65:223–240, 2015. https://doi.org/10.1007/s10236-014-0788-4.

Stull, R. B. *Practical meteorology: an algebra-based survey of atmospheric science* (University of British Columbia, 2015). https://www.eoas.ubc.ca/books/Practical_Meteorology/prmet/PracticalMet_WholeBook-v1_00b.pdf.

Sullivan, P. P. and McWilliams, J. C. Dynamics of winds and currents coupled to surface waves. *Annu. Rev. Fluid Mech*, 42:19–42, 2010. https://doi.org/10.1146/annurev-fluid-121108-145541.

Sullivan, P. P., McWilliams, J. C., and Moeng, C.-H. Simulation of turbulent flow over idealized waves. *J. Fluid Mech*, 404:47–85, 2000. https://doi.org/10.1017/S0022112099006965.

Sullivan, P. P., McWilliams, J. C., and Patton, E. G. Large-eddy simulation of marine atmospheric boundary layers above a spectrum of moving waves. *J. Atmos. Sci.*, 71:4001–4027, 2014. https://doi.org/10.1175/JAS-D-14-0095.1.

Taylor, G. I. Diffusion by continuous movements. *Proc. Lond. Math. Soc.*, 2 (1):196–212, 1922. https://doi.org/10.1112/plms/s2-20.1.196.

Thomson, W. On a disturbing infinity in Lord Rayleigh's solution for waves in a plane vortex stratum. *Nature*, 23 (45):188, 1880. https://www.nature.com/articles/023045a0.

Thykier-Nielsen, S., Deme, S., and Mikkelsen, T. Description of the atmospheric dispersion module rimpuff. *Riso National Laboratory, PO Box*, 49, 1999. https://www.researchgate.net/publication/228741276_Description_of_the_atmospheric_dispersion_module_RIMPUFF.

Versteeg, H. K. and Malalasekera, W. *An introduction to computational fluid dynamics: the finite volume method* (Pearson education, 2007).

Weideman, J. A. and Reddy, S. C. A matlab differentiation matrix suite. *ACM Trans. Math. Softw.*, 26 (4):465–519, 2000. ISSN 0098-3500. https://doi.org/10.1145/365723.365727.

Yang, D., Meneveau, C., and Shen, L. Dynamic modelling of sea-surface roughness for large-eddy simulation of wind over ocean wavefield. *J. Fluid Mech*, 726:62–99, 2013a. https://doi.org/10.1017/jfm.2013.215.

Yang, D., Shen, L., and Meneveau, C. An assessment of dynamic subgrid-scale sea-surface roughness models. *Flow, turbulence and combustion*, 91 (3):541–563, 2013b.

del Álamo, J. C. and Jimenez, J. Linear energy amplification in turbulent channels. *J. Fluid Mech*, 559:205–213, 2006. https://doi.org/10.1017/S0022112006000607.

About FFI

The Norwegian Defence Research Establishment (FFI) was founded 11th of April 1946. It is organised as an administrative agency subordinate to the Ministry of Defence.

FFI's mission

FFI is the prime institution responsible for defence related research in Norway. Its principal mission is to carry out research and development to meet the requirements of the Armed Forces. FFI has the role of chief adviser to the political and military leadership. In particular, the institute shall focus on aspects of the development in science and technology that can influence our security policy or defence planning.

FFI's vision

FFI turns knowledge and ideas into an efficient defence.

FFI's characteristics

Creative, daring, broad-minded and responsible.

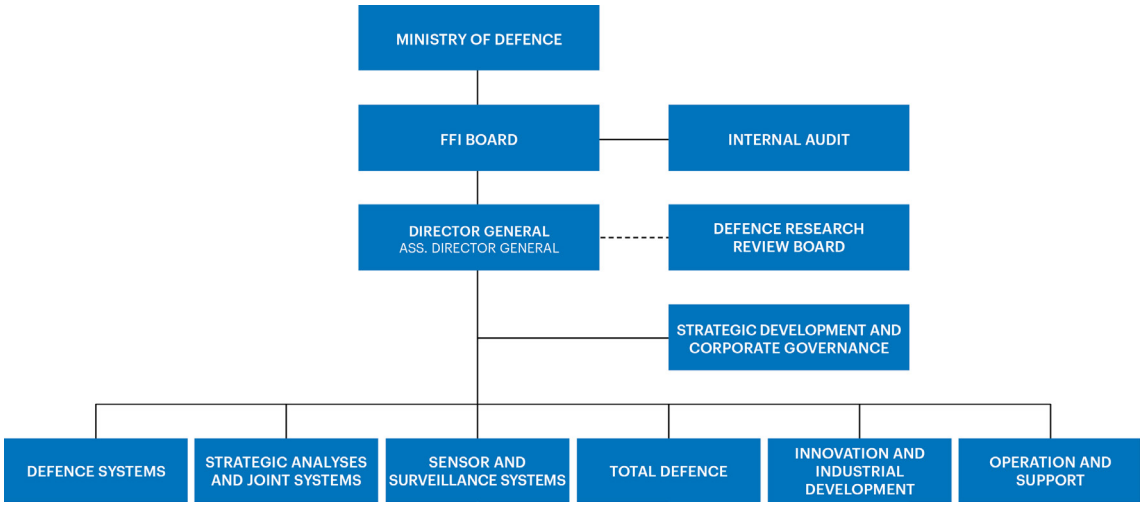

Forsvarets forskningsinstitutt (FFI)
Postboks 25
2027 Kjeller

Besøksadresse:
Kjeller: Instituttveien 20, Kjeller
Horten: Nedre vei 16, Karljohansvern, Horten

Telefon: 91 50 30 03
E-post: post@ffi.no
ffi.no

Norwegian Defence Research Establishment (FFI)
PO box 25
NO-2027 Kjeller
NORWAY

Visitor address:
Kjeller: Instituttveien 20, Kjeller
Horten: Nedre vei 16, Karljohansvern, Horten

Telephone: +47 91 50 30 03
E-mail: post@ffi.no
ffi.no/en